Operation of an Electrical Excited Synchronous Machine by Contactless Energy Transfer to the Rotor

Marcel Maier and Nejila Parspour

Abstract—**This paper deals with the design, the setup, and the operation of a rotating contactless energy transfer (CET) system. The system is used to replace the slip rings of an electrical excited synchronous machine and to transfer energy onto the rotor of the machine without mechanical contact. A compensation topology with an autoresonant circuit to generate the high frequency voltage is presented. Furthermore, the required parameters of the CET system are calculated. Based on these calculations, the system consisting of the power electronics, the compensation network, the magnetic path, the control system, and the electrical excited synchronous machine with controller, is set up. Finally, the calculated parameters are verified by measurements.**

Index Terms—**DC–AC power converters, electric machines, inductive power transmission, power electronics, resonant inverters, synchronous machines.**

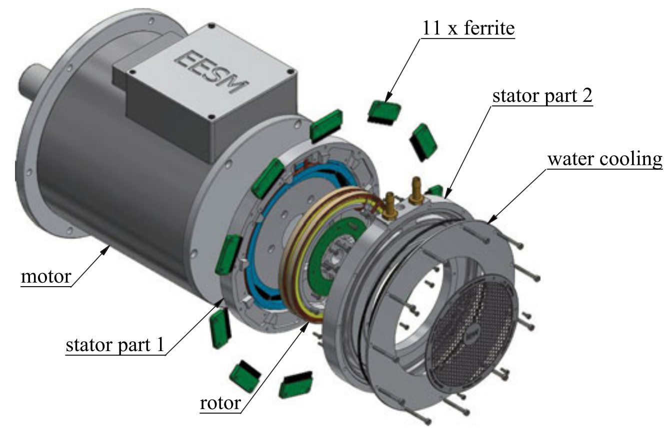

Fig. 1. Exploded view of a rotating contactless energy transfer system.

I. Introduction

During the electrification of the automotive technology, permanent magnet synchronous machines are the most contemplated type of traction drive. Beside a high torque and power density, permanent magnet synchronous machines also have several characteristics, which are not desired for the use in electric cars. The main common safety issue of permanent magnetic synchronous machines is the high induced voltage in the case of a lack of control over the power electronics in high speed operation [1]. A reasonable alternative to these machines are electrical excited synchronous machines, which use electromagnets to generate the rotor flux and offer a constant power operation over a wide speed range, by field weakening [2]–[5]. Mechanical slip rings offer a simple solution to conduct current onto the rotor field winding but maintenance and debris issues are unacceptable for many applications [6]–[8]. Compared to slip rings, rotating contactless energy transfer (CET) systems provide a reliable and maintenance-free solution [9]–[11].

In recent years, inductive power based CET systems have been established in many technical applications, e.g., to avoid plug connections or for rotating transformers [12], [13]. There are efforts to establish industrial standards like Qi from Wireless Power Consortium [14] for low power applications or WiPT for charging electrical vehicles [15]. Nevertheless, CET is still an important field of research [16]–[18].

Using a CET system instead of slip rings to operate an electrical excited synchronous machine (iEESM) implies some differences compared to well established applications, like battery charging or voltage stable power supply [19], [20]. The task of the CET-system, besides transferring energy to the rotor, is also to enable an accurate control of the rotor side excitation current. Due to high temperature and high rotational speed and associated high forces, it is advisable to avoid as many electronic parts on the rotor as possible. Hence, the current on the rotor has to be controlled using measured values and active components on the stator side. The CET system proposed in this paper does not contain ferrite parts for flux guidance or active electronics on the secondary side and therewith on the rotating part. Considering high temperature and high centrifugal forces this approach offers decisive advantages. Fig. 1 shows an exploded view of such a system. The first part of this paper shows the theoretical fundamentals of the proposed system. Then the transfer functions of a primary side serial, secondary side parallel compensated system (1s2p-system), and a primary side parallel, secondary side parallel compensated system (1p2p-system) are presented. Different possibilities of the arrangement of the compensation network are shown and evaluated for this use case. Furthermore, the parameters of the designed CET-system are calculated and the experimental setup on a test bench is described. At last, the experimental results are discussed and a conclusion is given.

Manuscript received September 4, 2017; revised February 23, 2018; accepted March 2, 2018. Date of publication March 9, 2018; date of current version July 17, 2018. Paper 2017-EMC-1050.R1, presented at the 17th International Conference on Power Electronics and Motion Control, Varna, Bulgaria, Sep. 25–30, 2016, and approved for publication in the IEEE Transactions on Industry Applications by the Electric Machines Committee of the IEEE Industry Applications Society. *(Corresponding author: Marcel Maier.)*

The authors are with the Institute of Electrical Energy Conversion, University of Stuttgart, Stuttgart 70569, Germany (e-mail: marcel.maier@iew.uni-stuttgart.de; parspour@iew.uni-stuttgart.de).

Color versions of one or more of the figures in this paper are available online at http://ieeexplore.ieee.org.

Digital Object Identifier 10.1109/TIA.2018.2814558

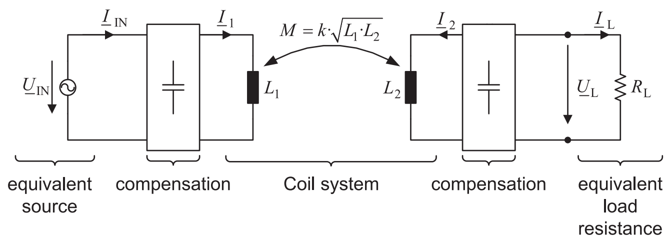

Fig. 2. Overview of a contactless energy transfer system from primary side equivalent source to secondary side equivalent load resistance.

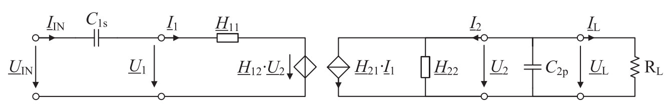

Fig. 3. Equivalent circuit of a 1s2p compensated system with H-parameters.

II. Basics of CET Systems

To calculate transfer functions and dimensions of the system, it is advantageous to simplify the equivalent circuit of a CET-system. Fig. 2 shows a simplified equivalent circuit with the coil-system, a compensation network on each side, an equivalent voltage source, which represents the power converter, and an equivalent load resistance [21]. The inverter and the rectifier are neglected. The input voltage of the CET-system $\underline{U}_{\mathrm{IN}}$ is modeled as an ideal sinusoidal voltage source [22]. Furthermore, the rectifier, the smoothing choke, and the load resistance on the secondary side are modeled by an equivalent load resistance R_{L}.

A. Topology of the CET-System

To transfer energy from one coil on the primary side to another coil on the secondary side, there are four different possibilities to arrange the compensation capacitors, assuming one capacitor on the primary side and one capacitor on the secondary side. Each capacitor can be connected in serial or in parallel to the coil. Due to the inductive load in electrical excited synchronous machines, a secondary side parallel compensation is advantageous. Hereby, the rectifier can be connected directly to the inductive load without a smoothing capacitor. In order to choose the compensation topology on the primary side, it is necessary to consider the transfer behavior. Both 1s2p-system and 1p2p-system allow us to control the current on the secondary side by using a measurement of the primary side current. The 1s2p-system is already calculated, set up, and tested in [20]. The advantage of a 1p2p-system is the possibility to use an autoresonant converter on the primary side. For our approach, a Royer converter with no need for any control was chosen. Furthermore, the 1p2p-system is safe against open and short circuit on the secondary side. This paper will compare the theory of both systems and present the calculation and measurements of the 1p2p-system.

B. 1s2p-System

Fig. 3 shows the equivalent circuit of a 1s2p-system. The use of controlled sources in the equivalent circuit of the coil system simplifies the calculation. Furthermore, it is advantageous to calculate the 1s2p-system with H-parameters [23]

$$\underline{H}_{11} = \mathrm{j}\omega L_1\left(1-k^2\right) \qquad \underline{H}_{12} = k\sqrt{\frac{L_1}{L_2}}$$
$$\underline{H}_{21} = -k\sqrt{\frac{L_1}{L_2}} \qquad \underline{H}_{22} = \frac{1}{\mathrm{j}\omega L_2}. \tag{1}$$

Based on the equivalent circuit shown in Fig. 3 and (1), the input impedance $\underline{Z}_{\mathrm{IN}}$ is calculated

$$\underline{Z}_{\mathrm{IN}} = \frac{\underline{U}_{\mathrm{IN}}}{\underline{I}_{\mathrm{IN}}} = \underbrace{\frac{1}{\mathrm{j}\omega C_{1\mathrm{s}}} + \mathrm{j}\omega L_1\left(1-k^2\right)}_{=\mathrm{j}X_1} + \frac{k^2\frac{L_1}{L_2}}{\underbrace{\frac{1}{\mathrm{j}\omega L_2} + \mathrm{j}\omega C_{2\mathrm{p}}}_{=\mathrm{j}B_2} + \frac{1}{R_{\mathrm{L}}}}. \tag{2}$$

Setting the reactance X_1 and the susceptance B_2 to zero leads to the following compensation capacities $C_{1\mathrm{s}}$ and $C_{2\mathrm{p}}$ [23]:

$$C_{1\mathrm{s}} = \frac{1}{\omega_0^2 L_1\left(1-k^2\right)} \qquad C_{2\mathrm{p}} = \frac{1}{\omega_0^2 L_2}. \tag{3}$$

In this design, there are up to three resonance frequencies, depending on the value of the equivalent load resistance R_{L}. Setting the imaginary part of $\underline{Z}_{\mathrm{IN}}$ to zero leads to these resonance frequencies and to the characteristic equivalent load resistance $R_{\mathrm{L,c}}$. Two resonance frequencies ω_{phL} and ω_{phH} exist only for equivalent load resistances greater than the characteristic equivalent load resistance $R_{\mathrm{L}} > R_{\mathrm{L,c}}$

$$\omega_{\mathrm{ph0}} = \omega_0 \qquad \omega_{\mathrm{phL}} < \omega_0 \qquad \omega_{\mathrm{phH}} > \omega_0 \tag{4}$$

$$R_{\mathrm{L,c}} = \omega_0 L_2\sqrt{\frac{1}{k^2}-1} \approx \frac{\omega_0 L_2}{k}. \tag{5}$$

Afterward the input impedance $\underline{Z}_{\mathrm{IN}}$, the voltage transfer function $M_{\mathrm{U}} = |\underline{U}_{\mathrm{L}}|/|\underline{U}_{\mathrm{IN}}|$ and the transadmittance $M_{\mathrm{Y}} = |\underline{I}_{\mathrm{L}}|/|\underline{U}_{\mathrm{IN}}|$ can be calculated for these resonant frequencies. This yields to (6)–(8) for ω_{ph0}

$$\underline{Z}_{\mathrm{IN}} = \frac{\underline{U}_{\mathrm{IN}}}{\underline{I}_{\mathrm{IN}}} = R_{\mathrm{L}} k^2 \frac{L_1}{L_2} \tag{6}$$

$$M_{\mathrm{U}} = \frac{|\underline{U}_{\mathrm{L}}|}{|\underline{U}_{\mathrm{IN}}|} = \frac{1}{k}\sqrt{\frac{L_2}{L_1}} \tag{7}$$

$$M_{\mathrm{Y}} = \frac{|\underline{I}_{\mathrm{L}}|}{|\underline{U}_{\mathrm{IN}}|} = \frac{1}{R_{\mathrm{L}} k}\sqrt{\frac{L_2}{L_1}} \tag{8}$$

and to (9)–(11) for ω_{phL} and ω_{phH}

$$\underline{Z}_{\mathrm{IN}} = \frac{\underline{U}_{\mathrm{IN}}}{\underline{I}_{\mathrm{IN}}} = \frac{\omega_0{}^2 L_1 L_2\left(1-k^2\right)}{R_{\mathrm{L}}} \tag{9}$$

$$M_{\mathrm{U}} = \frac{|\underline{U}_{\mathrm{L}}|}{|\underline{U}_{\mathrm{IN}}|} = \frac{R_{\mathrm{L}}}{\omega_0\sqrt{L_1 L_2\left(1-k^2\right)}} \tag{10}$$

$$M_{\mathrm{Y}} = \frac{|\underline{I}_{\mathrm{L}}|}{|\underline{U}_{\mathrm{IN}}|} = \frac{1}{\omega_0\sqrt{L_1 L_2\left(1-k^2\right)}}. \tag{11}$$

Fig. 4 shows the transfer functions, when driving the circuit with a stable resonance frequency, which is ω_{ph0}, ω_{phL}, and ω_{phH} for $R_{\mathrm{L}} \geq R_{\mathrm{L,c}}$ and ω_{ph0} otherwise.

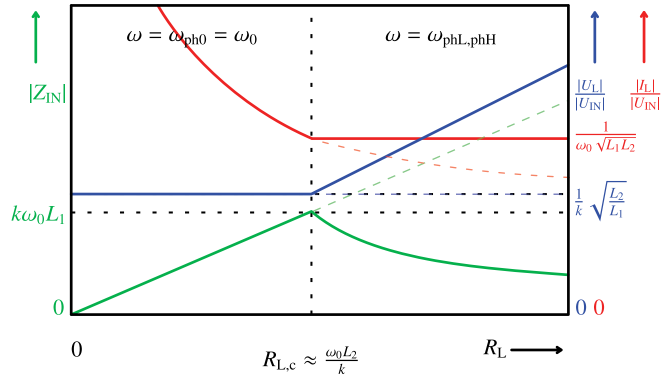

Fig. 4. Transfer function of a 1s2p compensated contactless energy transfer system.

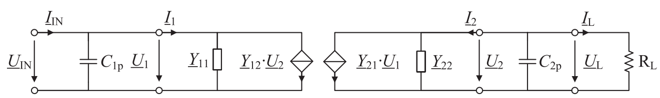

Fig. 5. Equivalent circuit of a 1p2p compensated system with Y-parameters.

C. 1p2p-System

Fig. 5 shows the equivalent circuit of a 1p2p-system.

It is advantageous to calculate the 1p2p-system with Y-parameters

$$\underline{Y}_{11} = \frac{1}{\mathrm{j}\omega L_1\left(1-k^2\right)} \qquad \underline{Y}_{12} = -\frac{k^2}{\mathrm{j}\omega M\left(1-k^2\right)}$$
$$\underline{Y}_{21} = -\frac{k^2}{\mathrm{j}\omega M\left(1-k^2\right)} \qquad \underline{Y}_{22} = \frac{1}{\mathrm{j}\omega L_2\left(1-k^2\right)}. \tag{12}$$

Based on the equivalent circuit shown in Fig. 5 and (12), the input admittance $\underline{Y}_{\mathrm{IN}}$ is calculated

$$\underline{Y}_{\mathrm{IN}} = \underbrace{\mathrm{j}\omega C_{1\mathrm{p}} + \frac{1}{\mathrm{j}\omega L_1\left(1-k^2\right)}}_{\stackrel{!}{=}\mathrm{j}B_1} + \frac{k^2}{\omega^2 L_1 L_2\left(1-k^2\right)^2}\cdot\frac{1}{\underbrace{\mathrm{j}\omega C_{2\mathrm{p}} + \frac{1}{\mathrm{j}\omega L_2\left(1-k^2\right)}}_{\stackrel{!}{=}\mathrm{j}B_2} + \frac{1}{R_{\mathrm{L}}}}. \tag{13}$$

Setting the susceptance B_1 and B_2 to zero, leads to the following compensation capacities $C_{1\mathrm{p}}$ and $C_{2\mathrm{p}}$:

$$C_{1\mathrm{p}} = \frac{1}{\omega_0^2 L_1\left(1-k^2\right)} \qquad C_{2\mathrm{p}} = \frac{1}{\omega_0^2 L_2\left(1-k^2\right)}. \tag{14}$$

In this design, there are up to three resonant frequencies, depending on the value of the equivalent load resistance R_{L}. Setting the imaginary part of $\underline{Y}_{\mathrm{IN}}$ to zero leads to these resonance frequencies and to the characteristic equivalent load resistance $R_{\mathrm{L,c}}$

$$\omega_{\mathrm{ph0}} = \omega_0 \qquad \omega_{\mathrm{phL}} < \omega_0 \qquad \omega_{\mathrm{phH}} > \omega_0 \tag{15}$$
$$R_{\mathrm{L,c}} = \frac{\omega_0 L_2\left(1-k^2\right)}{\sqrt{2-2\sqrt{1-k^2}}} \approx \frac{\omega_0 L_2}{k}. \tag{16}$$

Afterward the input impedance $\underline{Z}_{\mathrm{IN}}$, the voltage transfer function $M_{\mathrm{U}} = |\underline{U}_{\mathrm{L}}|/|\underline{U}_{\mathrm{IN}}|$ and the current transfer function $M_{\mathrm{I}} = \frac{|\underline{I}_{\mathrm{L}}|}{/}|\underline{I}_{\mathrm{IN}}|$ are calculated for these resonant frequencies. This yields to (17)–(19) for ω_{ph0}

$$\underline{Z}_{\mathrm{IN}} = \frac{\underline{U}_{\mathrm{IN}}}{\underline{I}_{\mathrm{IN}}} = \frac{\omega_0^2 L_1 L_2\left(1-k^2\right)^2}{R_{\mathrm{L}}\,k^2} \tag{17}$$
$$M_{\mathrm{U}} = \frac{|\underline{U}_{\mathrm{L}}|}{|\underline{U}_{\mathrm{IN}}|} = \frac{R_{\mathrm{L}}\,k}{\omega_0\sqrt{L_1 L_2}\left(1-k^2\right)} \tag{18}$$
$$M_{\mathrm{I}} = \frac{|\underline{I}_{\mathrm{L}}|}{|\underline{I}_{\mathrm{IN}}|} = \frac{\omega_0\sqrt{L_1 L_2}\left(1-k^2\right)}{R_{\mathrm{L}}\,k} \tag{19}$$

and to (20)–(22) for $\omega_{\mathrm{phL,phH}}$

$$\underline{Z}_{\mathrm{IN}} = \frac{\underline{U}_{\mathrm{IN}}}{\underline{I}_{\mathrm{IN}}} = R_{\mathrm{L}}\frac{L_1}{L_2} \tag{20}$$
$$M_{\mathrm{U}} = \frac{|\underline{U}_{\mathrm{L}}|}{|\underline{U}_{\mathrm{IN}}|} = \sqrt{\frac{L_2}{L_1}} \tag{21}$$
$$M_{\mathrm{I}} = \frac{|\underline{I}_{\mathrm{L}}|}{|\underline{I}_{\mathrm{IN}}|} = \sqrt{\frac{L_1}{L_2}}. \tag{22}$$

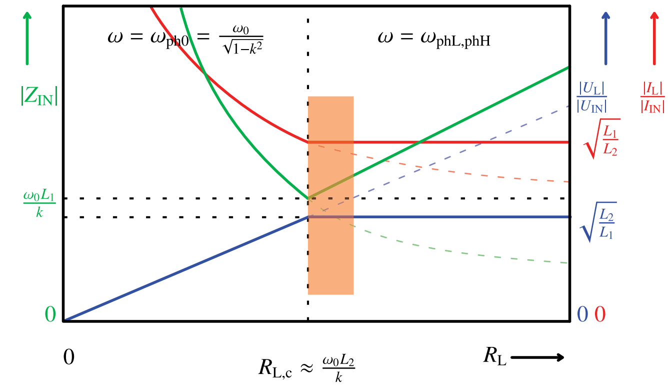

Fig. 6. Transfer function of a 1p2p compensated contactless energy transfer system.

Fig. 6 shows the curves, when driving the circuit with a stable resonance frequency, which is ω_{ph0}, ω_{phL}, and ω_{phH} for $R_{\mathrm{L}} \geq R_{\mathrm{L,c}}$ and ω_{ph0} otherwise.

D. Selection of a Topology

To define an operation range of the CET-system, first the topology of the primary side compensation network has to be chosen. Therefore, all requirements for the transfer behavior and the load have to be considered. It is advantageous to choose an operation range where the current transfer function $M_{\mathrm{I}} = \frac{|\underline{I}_{\mathrm{L}}|}{/}|\underline{I}_{\mathrm{IN}}|$ or the transadmittance $|M_{\mathrm{Y}}| = \frac{|\underline{I}_{\mathrm{L}}|}{/}|\underline{U}_{\mathrm{IN}}|$ are continuous over a variable equivalent load resistance R_{L}. The operation mode with a resonance frequency $\omega = \omega_{\mathrm{phL,phH}}$ at

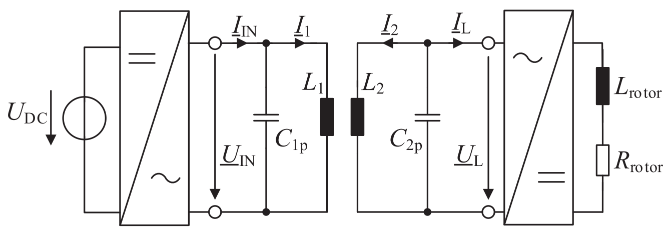

Fig. 7. Equivalent circuit of the complete system with the hf-inverter, the compensation network, the coil system, the rectifier, and the inductive load.

TABLE I
PARAMTERS OF THE iEESM AND BASIC PARAMETERS OF THE 1S2P PROTOTYPE

Parameter	Description	Value
$R_{\mathrm{rotor,min}}$	Resistance of the rotor of the iEESM at 20 °C	5 Ω
$R_{\mathrm{rotor,max}}$	Resistance of the rotor of the iEESM at 150 °C	8 Ω
k	Coupling factor between L_1 and L_2	0.47
$I_{\mathrm{rotor,max}}$	Maximum current in the iEESM	10 A
f_0	Design frequency	100 kHz
U_{DC}	Maximum voltage of the primary side dc link	112 V

the 1s2p-system and the operation mode with a frequency $\omega = \omega_{\mathrm{ph0}}$ at the 1p2p-system are matching the desired behavior of the transfer functions. The setup, calculation, and measurements of the 1s2p-system with a half-bridge inverter is already presented in [20]. Therefore, an inverter setup to drive the 1p2p-system is chosen [24] and will be investigated further. For a 1p2p-system, the equivalent load resistance R_{L} has to be greater than the characteristic equivalent load resistance $R_{\mathrm{L,c}}$, but as close to $R_{\mathrm{L,c}}$ as possible. If it differs too much, the maximum transferable power and the efficiency will decrease. The operation range is shown in Fig. 6.

Furthermore, it has to be considered that the equivalent load resistance of the system R_{L}, which is proportional to the resistance of the excitation winding R_{rotor}, depends on the temperature and can change during operation. But as the operation range has a hard lower limit and a soft upper limit, only the minimal temperature and thereby the minimal equivalent load resistance $R_{\mathrm{L,min}}$ has to be defined. This minimal temperature depends on the application area and has to be considered in the calculation.

III. System Design

Fig. 7 shows the equivalent circuit of the complete system and all necessary parameters, which are used to calculate the 1p2p-system. The equivalent circuit for the 1s2p-system is shown in [20].

A. Calculation of the 1s2p-System

To calculate the parameters of the CET-system, the parameters of the iEESM and other basic parameters are required (see Table I). The calculation of the 1s2p-system parameters is already shown in [20]. Table II shows an overview of all calculated parameters.

TABLE II
CALCULATED PARAMETERS OF THE CET-SYSTEM

Parameter	Description	Value
R_{L}	Resistance of the equivalent load at 20 °C	6.17 Ω
R_{L}	Resistance of the equivalent load at 150 °C	9.87 Ω
$\lvert I_{\mathrm{L,max}}\rvert$	Absolute value of the maximum equivalent current	9 A
$\lvert U_{\mathrm{IN}}\rvert$	Absolute value of the maximum equivalent input voltage	100 V
L_2	Secondary side inductance	5.25 μH
L_1	Primary side inductance	79.6 μH

TABLE III
PARAMTERS OF THE iEESM AND BASIC PARAMETERS OF THE 1P2P PROTOTYPE

Parameter	Description	Value
k	Coupling factor between L_1 and L_2	0.33
I_{DC}	Maximum current of the primary side dc link	10 A

B. Calculation of the 1p2p-System

To calculate the parameters of the 1p2p-system, some additional parameters to the parameters in table I are required (see Table III).

1) Equivalent Load Resistance: The transmission ratio between the equivalent load resistance R_{L} and the actual resistance of the rotor of the iEESM R_{rotor} depends on the topology of the rectifier and the compensation topology. For the described CET-system with a secondary side parallel compensation, a full-wave rectifier with the following transmission ratio is established [18]:

$$R_{\mathrm{L}} = R_{\mathrm{rotor}} \frac{\pi^2}{8} \approx \frac{1}{0.81} \cdot R_{\mathrm{rotor}}. \tag{23}$$

2) Equivalent Output Current: The transmission ratio between the equivalent current I_{L} and the current of the rotor of the iEESM I_{rotor} depends both on the topology of the rectifier and the compensation. It is calculated using the transmission ratio of the resistances

$$I_{\mathrm{L}} = I_{\mathrm{rotor}} \frac{\sqrt{8}}{\pi} \approx 0.9 \cdot I_{\mathrm{rotor}}. \tag{24}$$

3) Equivalent Input Voltage: The transmission ratio between the equivalent voltage U_{IN} and the dc-link voltage U_{DC} depends on the topology of the inverter and the compensation. For this CET-system with a primary side parallel compensation, a Royer converter with the following transmission ratio is established [23]:

$$I_{\mathrm{IN}} = I_{\mathrm{DC}} \frac{\sqrt{2}}{\pi}. \tag{25}$$

4) Secondary Side Inductance: According to (16), the constant coupling factor k and the constant design frequency ω_0, the inductance of the secondary side coil L_2 directly affects the characteristic equivalent load resistance R_{L}. To meet the optimal operation range as shown in Fig. 6, the secondary side inductance L_2 is calculated by transforming (16)

$$L_2 = \frac{R_{\mathrm{L,c}} \sqrt{2 - 2\sqrt{1-k^2}}}{\omega_0 \left(1-k^2\right)} \leq \frac{R_{\mathrm{L}} \sqrt{2 - 2\sqrt{1-k^2}}}{\omega_0 \left(1-k^2\right)}. \tag{26}$$

TABLE IV
CALCULATED PARAMETERS OF THE CET-SYSTEM

Parameter	Description	Value
R_{L}	Resistance of the equivalent load at 20 °C	6.17 Ω
R_{L}	Resistance of the equivalent load at 150 °C	9.87 Ω
$\lvert I_{\mathrm{L,max}}\rvert$	Absolute value of the maximum equivalent current	9 A
$\lvert U_{\mathrm{IN}}\rvert$	Absolute value of the maximum equivalent input voltage	222 V
L_2	Secondary side inductance	3.98 μH
L_1	Primary side inductance	15.92 μH

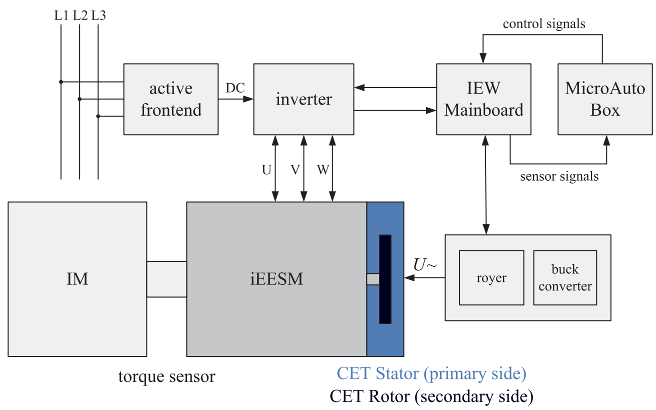

Fig. 8. Components of the test bench with the electrical excited synchronous machine and the contactless energy transfer system.

5) Primary Side Inductance: The inductance of the primary coil is found using (22)

$$L_1 = \frac{|\underline{I}_{\mathrm{L}}|^2}{|\underline{I}_{\mathrm{IN}}|^2} L_2. \tag{27}$$

6) Overview of the Calculated Parameters: Table IV shows the calculated parameters.

IV. EXPERIMENTAL SETUP

To verify the operation of an iEESM, the CET-system was constructed and adapted to an electrical excited synchronous machine and put in operation on a test bench for electrical machines. Fig. 8 shows an overview of all components of this test bench. The iEESM is coupled with an induction machine. The three stator phases of the iEESM are fed by a six pulse inverter. The insulated gate bipolar transistors are controlled by a pulse-width modulated voltage signal with up to 18 kHz switching frequency. The 600 V dc power supply is provided by an active front end, connected to the three phase grid. The control algorithm for the field oriented control of the iEESM is done in MATLAB/Simulink and built in a digital signal processor of the rapid prototyping environment MicroAutoBox II by dSPACE. Malfunction monitoring and analog signal detection is done with complex programmable logic device-based signal and safety electronics, developed at the Institute of Electrical Energy Conversion, University of Stuttgart (IEW Mainboard). As explained in Section III, the CET-system has a Royer converter on the primary side and a full bridge rectifier on the secondary side. The input current I_{DC} and therewith the rotor current I_{rotor} is controlled by a buck converter connected to the input pins of the Royer converter.

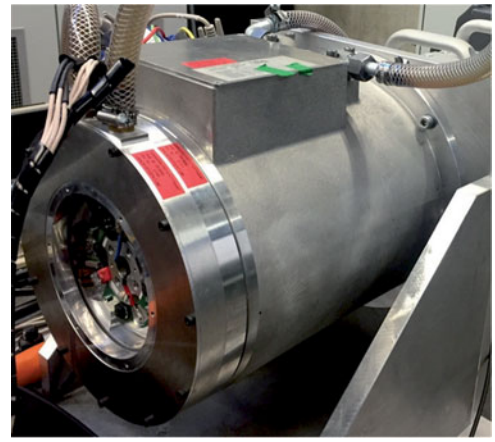

Fig. 9. Electrical excited synchronous machine with adapted CET-system.

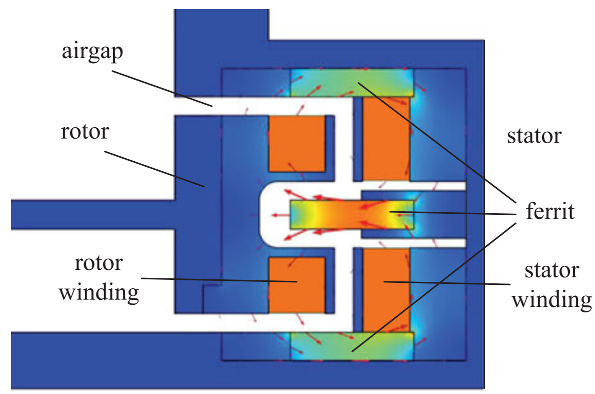

Fig. 10. Magnetic flux density path simulated in an FEM tool.

A. Electrical Excited Synchronous Machine

Fig. 9 shows the electrical excited synchronous machine with the adapted CET-system. The electrical machine has a power output of about 60 kW and a maximum rotational speed of about 10 000 rpm.

B. Magnetic Path

Fig. 10 shows the draft of the magnetic path with the housing, the soft magnetic ferrite, nonmagnetic materials for mechanical reasons and the rotor and stator windings. Using finite element method (FEM) simulations in two-dimensional (2-D) and 3-D, the geometry and the dimension were optimized for the 1p2p CET-system. Compared to the 1s2p prototype, presented in [20], the dimensions of the active part of the energy transfer system could be reduced by about half. Although, this reduction leads to higher eddy current losses in the aluminum, the advantages of the smaller dimensions dominate in this purpose. Fig. 11 shows the cross-sectional view of the optimized geometry.

Due to the high rotational speed, a construction without ferrite material on the rotor is developed. To protect the rotor coil against the centrifugal force, a glass fiber bandage is wrapped around the coil and both, the coil and the glass fiber bandage, are

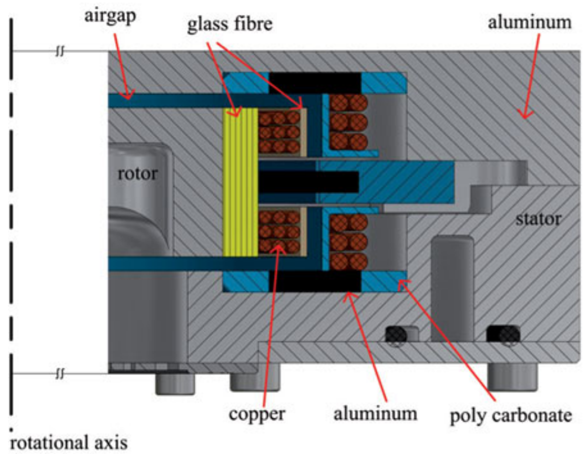

Fig. 11. Section view of the optimized geometry, including the coils, the ferrite, the aluminum shielding, and the nonconducting carrier material.

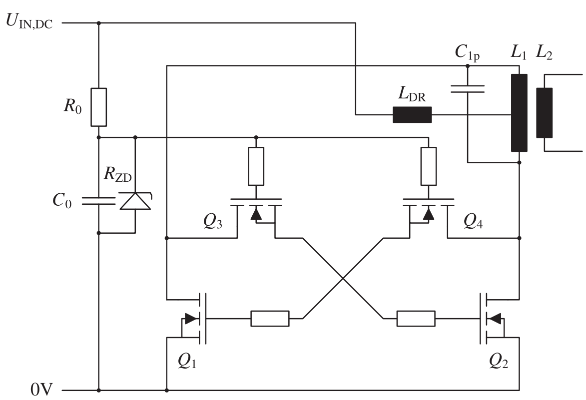

Fig. 12. Royer converter with MOSFETs.

potted in epoxy resin. Therewith, the rotor consists only of an aluminum pulley and a potted construction of copper and glass fiber.

C. Power Electronics of the CET-System

On the primary side, a Royer converter converts direct voltage in alternating voltage. The circuit works autoresonant with a resonance frequency, defined by the capacitor $C_{1\mathrm{p}}$, the inductance L_1, and the coupled secondary side magnetic path. For the first time, the circuit was developed and patented in 1954 by George Howard Royer and Richard Louis Bright [25]. An improved highly efficient variant is shown in Fig. 12 [24].

Due to the zero current switching and the high efficient gate triggering using MOSFETs, this converter can reach very high overall efficiencies. The coil with center tap L_1 is serving as the primary side of the transmission path for the CET-system. The capacitor $C_{1\mathrm{p}}$ is connected in parallel. The resonance frequency of the parallel resonant circuit is also the frequency for energy transfer and can be designed by varying the capacity. Basically, the Royer converter with high efficient gate triggering consists of four MOSFETs (Q_1, Q_2, Q_3, Q_4). The MOSFETs Q_1 and Q_2 drive the active power of the system and the MOSFETs Q_3 and Q_4 provide the high efficient gate triggering of Q_1 and Q_2. The source pins of Q_1 and Q_2 are always connected to ground. The inductor L_{DR} forms, in combination with a buck converter, the constant current source. Therefore, L_{DR} should be at least ten times bigger than L_1. The buck converter can be used to control either the input voltage or the input current of the Royer converter. Fig. 13 shows the connection of the buck converter and the Royer converter. To optimize the system and reduce the amount of electronic components, the inductance L_{DR} is used both as current source for the Royer converter and as an inductor for the buck converter. Fig. 14 shows the circuit board of the buck converter, connected to the IEW Mainboard with a fiber optic cable and the Royer converter.

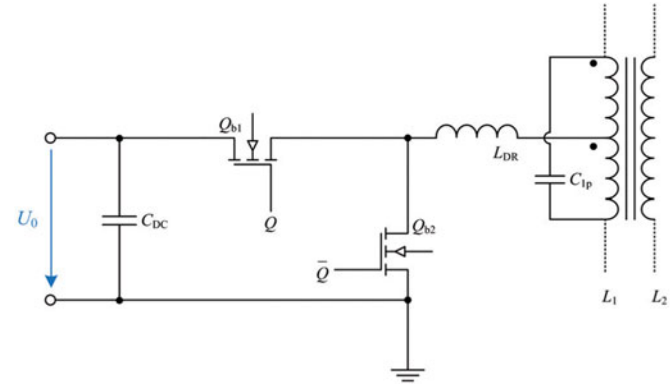

Fig. 13. Buck converter combined with Royer converter.

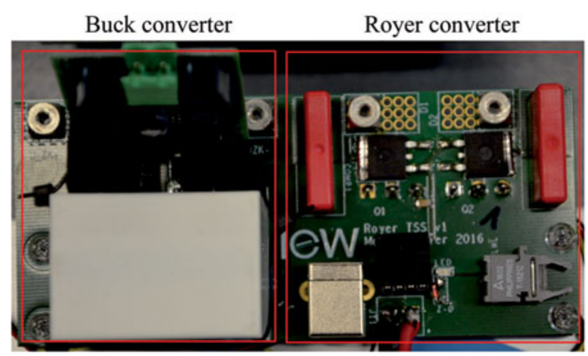

Fig. 14. Buck converter and Royer converter.

V. Measurement and Results

To demonstrate that the inductance L_{DR} can be used as an inductor for the buck converter and as a current source for the Royer converter, Fig. 15 shows a measurement of the output voltage of the buck converter U_{DC} and the voltage of the parallel resonance circuit $U_{\mathrm{C}_{1\mathrm{p}}}$. One can see that the voltage of the parallel resonance circuit $U_{\mathrm{C}_{1\mathrm{p}}}$ is hardly affected by the switching state of the buck converter.

Fig. 16 shows the transmission ratio of the output voltage U_{L} and the input voltage U_{IN}. The measured voltage transfer function is matching the ideal voltage transfer function, deduced in Section II-C, very well. The deviation is caused by losses in the system. Simplified, the losses can be divided into serial loss resistances and parallel loss resistances. The deviation in the voltage transfer function is only affected by serial loss resistances, e.g., voltage drop of diodes. To explain the measurement

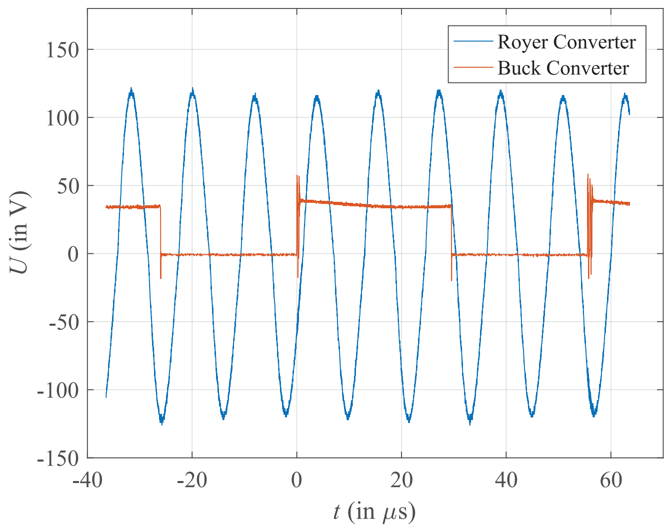

Fig. 15. Measurement of the voltage of the buck converter and the voltage of the royer capacitor.

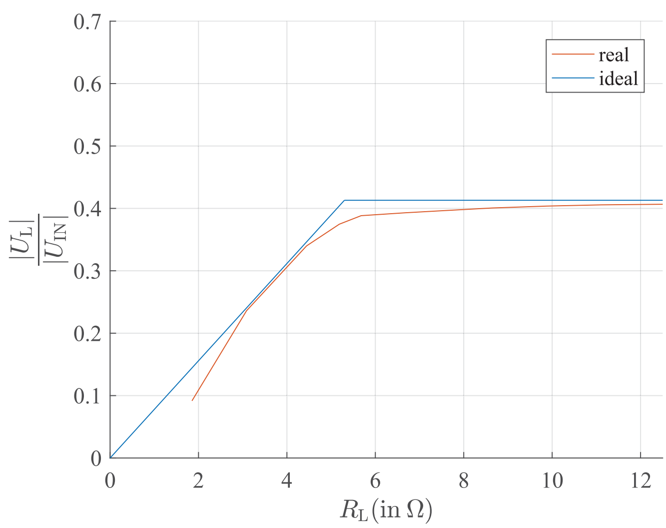

Fig. 16. Transmission ratio of the output voltage U_{L} and the input voltage U_{IN}.

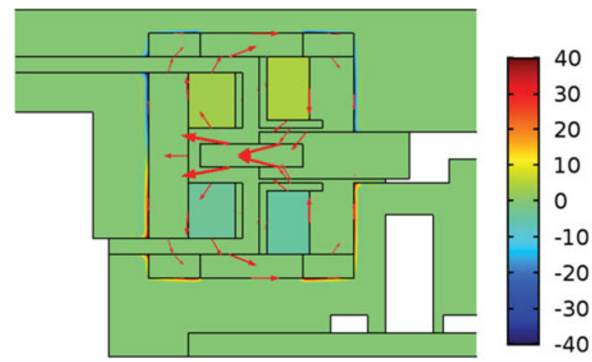

Fig. 17. Result of 2-D magnetic field simulation—Surface: Current density, phi component [A/mm^2], Arrow Line: Magnetic flux density.

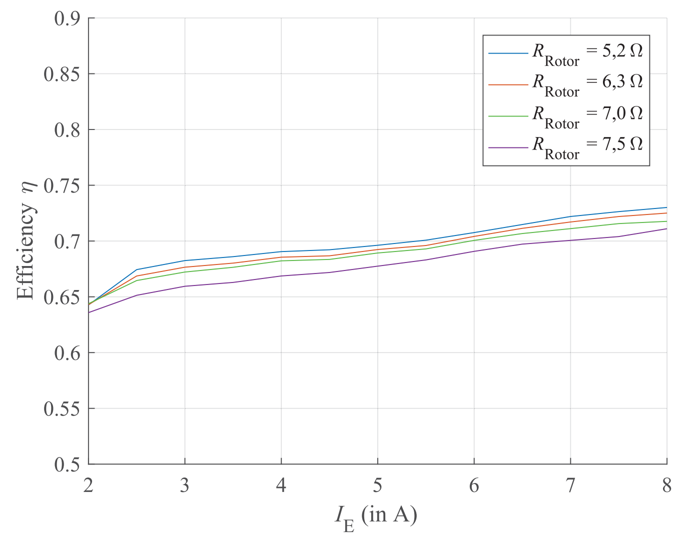

Fig. 18. Overall efficiency of the CET-system.

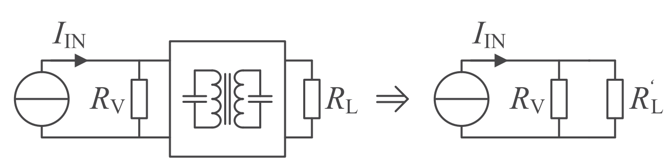

Fig. 19. Simplified equivalent circuit with the parallel loss resistance R_{V}.

of the efficiency of the system, an FEM-Simulation of the system was done [26] and the current density of the simulation is shown in Fig. 17. As Fig. 17 shows, there is a current density unequal to zero in the coils and in the aluminum. Due to the ferrite free rotor and the reduction of the dimension of the magnetic path, not negligible current densities and therewith losses occur in the aluminum parts.

Fig. 18 shows the overall efficiency of the CET-system for different rotor resistances R_{rotor}, which is, as expected, lower than it would be possible with smaller eddy current losses in the aluminum.

Regarding the rated power of 40 kW of the electrical excited synchronous machine (EESM) the losses of about 100 W have a very small influence on the efficiency of the EESM, but the losses influence the transmission behavior of the CET-system. The eddy current losses and the copper losses of the parallel resonant circuit are modeled as a parallel loss resistance R_{V} on the primary side (see Fig. 19).

Due to a constant current transfer function $M_{\mathrm{I}} = \sqrt{\frac{L_1}{L_2}}$ for $\omega = \omega_{\mathrm{phL,phH}}$, the equivalent load resistance R_{V} is converted to a primary side resistance $R_{\mathrm{L}}' = M_{\mathrm{I}}^2 R_{\mathrm{L}}$. The loss resistance R_{V} was measured with a LCR-meter and is $R_{\mathrm{V}} = 180\ \Omega$. Considering this simplified loss model and the measured parallel loss resistance R_{V}, the current transfer function M_{I} is adapted to

$$M_{\mathrm{I,R_V}} = \frac{R_{\mathrm{V}}}{R_{\mathrm{V}} + R_{\mathrm{L}}'} M_{\mathrm{I}}. \tag{28}$$

Fig. 20 shows the transmission ratio of the output current I_{L} to the input current I_{IN} depending on the equivalent load resistance R_{L}.

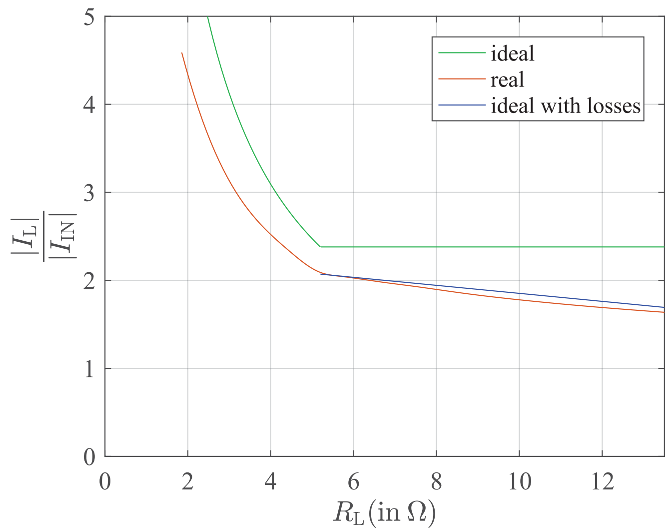

Fig. 20. Transmission ratio of the output current I_L and the input voltage U_{IN}.

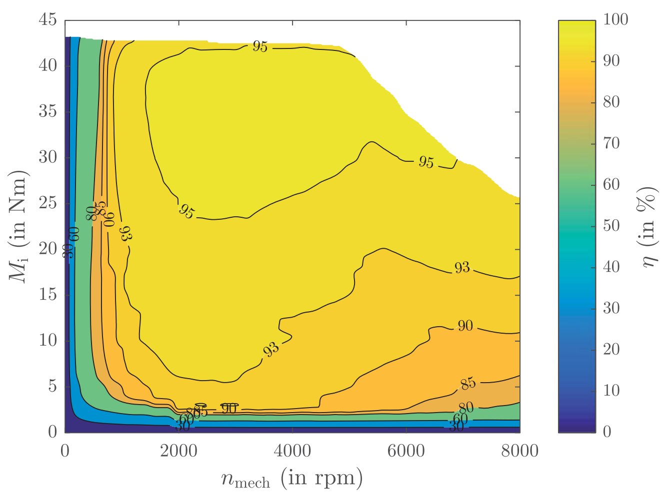

Fig. 21. Overall efficiency of the iEESM.

One can see, that the measured transfer function is matching the ideal transfer function with losses very well. To prove the low influence of the efficiency of the CET-system, the overall efficiency of the iEESM was measured and is shown in Fig. 21.

VI. Conclusion

In order to evaluate the performance of an electrical excited synchronous machine with CET to the rotor, the design, the setup, and measurements of such an iEESM are shown. First of all, the transfer behaviors of a 1s2p-system and a 1p2p-system are discussed and the optimal operation ranges of those systems are defined. Furthermore, the parameters for the 1p2p CET-system depending on the parameters of an iEESM are calculated and a magnetic path and power electronics are built. In the final step, the complete system is set up on a test bench and measurements for the switching behavior, the transmission ratio, the efficiency of the CET-system, and the overall efficiency of the iEESM are made. One can see that a system using only one inductor for a buck converter and a Royer converter is working very well. Furthermore, the measured transmission ratios of the CET-system are matching very well to the theoretically calculated ratios. Therewith, a rotating CET-system with many advantages over conventional solutions was built and tested. As the rotor is without ferrite parts, it can be built very stable and easy to balance. Due to the segmented construction of the flux leading material, the dimension and the rated power can be varied easily. Overall, it is shown that this novel rotating CET-system offers the possibility of using inductive electrical excited synchronous machines for electrical vehicles.

References

[1] S. Estenlund, M. Alakula, and A. Reinap, "Pm-less machine topologies for EV traction: A literature review," in *Proc. Int. Conf. Elect. Syst. Aircr., Railway, Ship Propulsion, Road Veh, Int. Transp. Electrif. Conf.*, 2016, pp. 1–6.

[2] I. Boldea, L. N. Tutelea, L. Parsa, and D. Dorrell, "Automotive electric propulsion systems with reduced or no permanent magnets: An overview," *IEEE Trans. Ind. Electron.*, vol. 61, no. 10, pp. 5696–5711, Oct. 2014.

[3] W. Q. Chu, Z. Q. Zhu, and J. T. Chen, "Simplified analytical optimization and comparison of torque densities between electrically excited and permanent-magnet machines," *IEEE Trans. Ind. Electron.*, vol. 61, no. 9, pp. 5000–5011, Sep. 2014.

[4] M. L. Bash and S. D. Pekarek, "Modeling of salient-pole wound-rotor synchronous machines for population-based design," *IEEE Trans. Energy Convers.*, vol. 26, no. 2, pp. 381–392, Jun. 2011.

[5] J. Jurgens, A. Brune, and B. Ponick, "Electromagnetic design and analysis of a salient-pole synchronous machine with tooth-coil windings for use as a wheel hub motor in an electric vehicle," in *Proc. Int. Conf. Elect. Mach.*, 2014, pp. 744–750.

[6] H. Ma, T. Chen, Y. Zhang, P. Ju, and Z. Chen, "Research on the fault diagnosis method for slip ring device in doubly-fed induction generators based on vibration," *IET Renewable Power Gener.*, vol. 11, no. 2, pp. 289–295, 2017.

[7] A. T. Hermann Houenouvo and W. Hofmann, "Diagnostics of the transmission properties of the slip ring system in doubly fed induction generators," in *Proc. IEEE 60th Holm Conf. Elect. Contacts*, 2014, pp. 1–7.

[8] A. T. H. Houenouvo and W. Hofmann, "Finite element analysis of the contact problem between graphite-brushes and — slip rings in double-fed asynchronous generators," in *Proc. 9th Int. Multi-Conf. Syst., Signals Devices*, 2012, pp. 1–6.

[9] J.-N. Weber, A. Rehfeldt, S.-A. Vip, and B. Ponick, "Rotary transformer with electrical steel core for brushless excitation of synchronous machines," in *Proc. 22nd Int. Conf. Elect. Mach.*, 2016, pp. 884–889.

[10] D. Bortis, L. Fassler, A. Looser, and J. W. Kolar, "Analysis of rotary transformer concepts for high-speed applications," in *Proc. 28th Annu. IEEE Appl. Power Electron. Conf. Expo.*, 2013, pp. 3262–3269.

[11] C. Stancu, T. Ward, K. Rahman, R. Dawsey, and P. Savagian, "Separately excited synchronous motor with rotary transformer for hybrid vehicle application," in *Proc. IEEE Energy Convers. Congr. Expo.*, 2014, pp. 5844–5851.

[12] J. Smeets, D. Krop, J. W. Jansen, M. Hendrix, and E. A. Lomonova, "Optimal design of a pot core rotating transformer," in *Proc. IEEE Energy Convers. Congr. Expo.*, 2010, pp. 4390–4397.

[13] K. D. Papastergiou and D. E. Macpherson, "An airborne radar power supply with contactless transfer of energy—part i: Rotating transformer," *IEEE Trans. Ind. Electron.*, vol. 54, no. 5, pp. 2874–2884, Oct. 2007.

[14] A. Berger, M. Agostinelli, C. Sandner, S. Vesti, and M. Huemer, "High efficient integrated power receiver for a Qi compliant wireless power transfer system," in *Proc. IEEE Wireless Power Transfer Conf.*, 2016, pp. 1–4.

[15] O. Simon, J. Mahlein, F. Turki, D. Dorflinger, and A. Hoppe, "Field test results of interoperable electric vehicle wireless power transfer," in *Proc. 18th Eur. Conf. Power Electron. Appl.*, 2016, pp. 1–10.

[16] M. Zimmer, J. Heinrich, and N. Parspour, "Design of a 3 kw primary power supply unit for inductive charging systems optimized for the compatibility to receiving units with 20 kw rated power," in *Proc. 4th Int. Elect. Drives Prod. Conf.*, 2014, pp. 1–5.

[17] S. Li and C. C. Mi, "Wireless power transfer for electric vehicle applications," *IEEE J. Emerg. Sel. Topics Power Electron.*, vol. 3, no. 1, pp. 4–17, Mar. 2015.
[18] R. Bosshard, J. W. Kolar, J. Muhlethaler, I. Stevanovic, B. Wunsch, and F. Canales, "Modeling and eta-alpha-pareto optimization of inductive power transfer coils for electric vehicles," *IEEE J. Emerg. Sel. Topics Power Electron.*, vol. 3, no. 1, pp. 50–64, Mar. 2015.
[19] M. Maier, M. Zimmer, J. Heinrich, D. Maier, and N. Parspour, "Dimensioning of a contactless energy transfer system for an electrical excited synchronous machine," in *Proc. IEEE Wireless Power Transfer Conf.,* 2016, pp. 1–3.
[20] M. Maier and N. Parspour, "Operation of an electrical excited synchronous machine by contactless energy transfer to the rotor," in *Proc. IEEE Int. Power Electron. Motion Control Conf.*, 2016, pp. 625–630.
[21] N. Parspour, J. Heinrich, P. Seitz, and M. Zimmer, "Development of positioning tolerant inductive charging systems for electric vehicles," in *Proc. 3rd Int. Elect. Drives Prod. Conf.*, 2013, pp. 426–430.
[22] R. L. Steigerwald, "A comparison of half-bridge resonant converter topologies," *IEEE Trans. Power Electron.*, vol. 3, no. 2, pp. 174–182, Apr. 1988.
[23] D. Maier, J. Heinrich, M. Zimmer, M. Maier, and N. Parspour, "Contribution to the system design of contactless energy transfer systems," in *Proc. IEEE Int. Power Electron. Motion Control Conf.*, 2016, pp. 1008–1013.
[24] M. Maier, D. Maier, M. Zimmer, and N. Parspour, "A novel self oscillating power electronics for contactless energy transfer and frequency shift keying modulation," in *Proc. 2016 Int. Symp. Power Electron., Elect. Drives, Autom. Motion.*, 2016, pp. 67–72.
[25] R. L. Bright, G. H. Royer, "Electrical inverter circuits," 1957. [Online]. Available: http://www.google.com/patents/US2783384
[26] M. Maier, M. Hagl, M. Zimmer, J. Heinrich, and N. Parspour, "Design and construction of a novel rotating contactless energy transfer system for an electrical excited synchronous machine," in *Proc. 22nd Int. Conf. Elect. Mach.*, 2016, pp. 709–714.

Marcel Maier received the Dipl. Ing. degree in electrical engineering and information technology. He was born on June 26, 1986, in Heidelberg, Germany. He graduated from the secondary school, Sindelfingen, Germany, and studied electrical engineering at the University of Stuttgart, Stuttgart, Germany.

Since 2012, he has been with the Institute of Electrical Energy Conversion, University of Stuttgart. His research interest focuses on rotating contactless energy transfer systems for electrical excited synchronous machines.

Nejila Parspour received the Master's and the Ph.D. (*summa cum laude*) degrees in electrical engineering from the Technical University of Berlin, Berlin, Germany, in 1991 and 1995, respectively.

She is currently a Professor in electrical energy conversion with the University of Stuttgart, Stuttgart, Germany, and the Head of the Institute of Electrical Energy Conversion. Before joining the University of Stuttgart, she was with the Philips for five years and six years with the University of Bremen. Her research and teaching interests include electrical machines and drives with a focus on machine design and in the field of contactless energy transfer with a focus on inductive charging systems.